INTERNATIONAL JOURNAL OF
COASTAL, OFFSHORE & ENVIRONMENTAL ENGINEERING IJCOE Vol. 11/No. 4/Autumn 2026 (91-101)

Available online at: www. Ijcoe.org

Sensitivity Analysis of Wave and Current in Numerical Modeling and Comparison with Field Measurements During Small Storms in Northern Ports of Iran

Rasul Koohzad[1], Reza Dezvareh[2*]

[1] *MSc Student, Faculty of Civil Engineering, Babol Noshirvani University of Technology, Babol, Iran,.rasulkoohzad@gmail.com*
[2*] *Associate Professor, Faculty of Civil Engineering, Babol Noshirvani University of Technology, Babol, Iran, rdezvareh@nit.ac.ir*

ARTICLE INFO

Article History:
Received: 18 Aug
Accepted: 24 Nov
Available online ….

Keywords:
Hydrodynamics
Caspian Sea
Flow Model
Nowshahr
Mike 21

ABSTRACT

This study conducts a sensitivity analysis of wave and current behavior during minor storms along the southern coast of the Caspian Sea, focusing on the port of Nowshahr, a significant maritime hub in northern Iran. Using MIKE21, a numerical modeling software, the analysis evaluates various parameters such as mesh size, angular divisions, bed roughness, and wave breaking coefficients. The numerical models were calibrated and validated by comparing their outputs with field measurements obtained during small storm events. Results indicate that certain parameters, such as computational grid size and wave breaking coefficients, significantly influence model accuracy, while others, such as angular divisions, have minimal impact. Wind data from ECMWF-ERA5 was used to simulate local conditions accurately. The findings provide insights into optimizing numerical model calibration for improved predictions of wave and current behavior, particularly under storm conditions, thereby supporting coastal engineering projects and enhancing understanding of marine hydrodynamics in this region.

1. Introduction

Sensitivity analysis refers to studying how variations in input variables of a statistical model can affect its output. In other words, it is a systematic way to modify a model's inputs and predict the corresponding effects on its results [1]. Sensitivity analysis is crucial for making accurate use of numerical models through various software programs. Given the high level of uncertainty in marine environments, this analysis becomes even more important [2]. Since waves and currents are key factors in marine environments, many researchers have conducted sensitivity analyses on these two parameters. In 2010, Beels et al. performed a sensitivity analysis on wave energy absorber numerical modeling [3]. In 2013, DAO et al. analyzed tsunami waves through a Reynolds-Averaged Navier-Stokes (RANS) based numerical model, assessing the effect of coastal parallel channels on tsunami wave energy reduction [4]. In 2015, Nekouee et al. conducted a sensitivity analysis on wave prediction numerical models considering wind and geometry effects [5]. In 2016, Bastidas et al. simulated artificial storm tracks using Delft 3D software and carried out sensitivity analyses to estimate storm hazards in the absence of experimental wave and coastal wave observations [6]. Liu and Guo, in 2018, applied sensitivity analysis to study the combined effects of waves and currents on risers [7]. Moreover, Zhen et al., in 2021, conducted a sensitivity analysis on wave direction for three cases: external channel excavation, wave, and storm in a shielded port [8]. Their findings suggest that wave direction sensitivity is stronger near the entrance of ports with an excavated external channel. Based on this, it was recommended that primary wave direction analysis be carried out.

It is worth mentioning that, in addition to the sensitivity analysis briefly reviewed in the literature, other researchers have employed artificial intelligence-based methods, such as neural networks [10,11], machine learning [12], and support vector machines [13, 14], to better analyze numerical model data and compare them with field measurements. Building upon these studies, the aim of the present paper is to conduct a sensitivity analysis of waves and currents using MIKE software and to compare the results with field measurements during minor storms along the southern coast of the

Caspian Sea in northern Iran. For this purpose, the area surrounding the port of Nowshahr, one of the most significant and longstanding ports in northern Iran, has been selected as the study area.

2. Materials and Methods

This section presents the details of the numerical models developed for the study area. It is worth noting that MIKE21, a software package developed by the Danish Hydraulic Institute (DHI), was used for modeling in this study. MIKE21 is one of the most reliable and widely used numerical simulators for hydrodynamic modeling of aquatic environments [15].

2.1. Large-Scale Wave and Current Modeling

For simulating the hydrodynamic phenomena of the southern coasts of the Caspian Sea, it is necessary to first simulate the marine wave and current conditions in this region. The local wave and current conditions are not independent of the conditions in the entire Caspian Sea. Therefore, for local hydrodynamic modeling, the boundary conditions of marine waves and currents at the open borders of the local model must be determined.

2.2. Mesh Gridding for Wave Model

The simulation area includes the entire Caspian Sea. Bathymetric data and depth variations for this area are provided below. Figure 1 shows the coastal line. The continuous red line represents data obtained from Google Earth. It is important to note the non-synchronicity of Google Earth maps when determining the coastal line.



Figure 1. Comparison of available sources for coastal line representation. The continuous red line represents data obtained from Google Earth, the white markers indicate data from the NASA website, and the red markers show data gathered from the Caspian Sea Environmental Program.

Wind is the most important factor in wave generation in seas. Therefore, accurate wave modeling requires wind data with suitable temporal and spatial resolution. Figure 2 shows the wind rose derived from ECMWF-ERA5 data at a deep-water location in front of the study area. Considering the alignment between the wind rose obtained from ERA5 data and the hydrodynamic conditions of the region, and given the superior temporal and spatial accuracy of this data compared to other available wind fields, these data were used for further simulations.

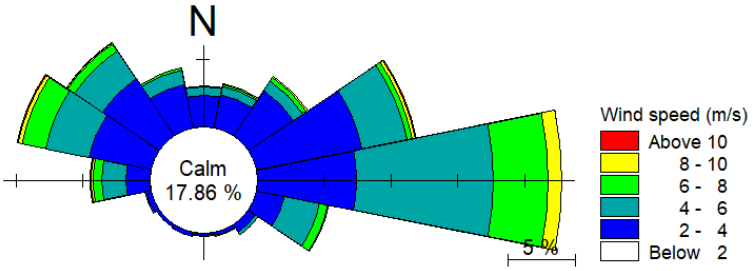


Figure 2. Wind rose obtained from ECMWF-ERA5 data

2.3. Wave and Current Measurements

To understand the overall wave patterns based on measured field data, Figure 3 presents the wave rose for the measured data at Nowshahr. As shown, the predominant wave direction in the region is from the northwest, which has the longest fetch. Based on this figure, it can be predicted that due to the angle of wave incidence relative to the coastline, wave breaking in the surf zone will cause the dominant currents generated by wave breaking to flow from west to east. Consequently, sediment transport will also be predominantly west to east.

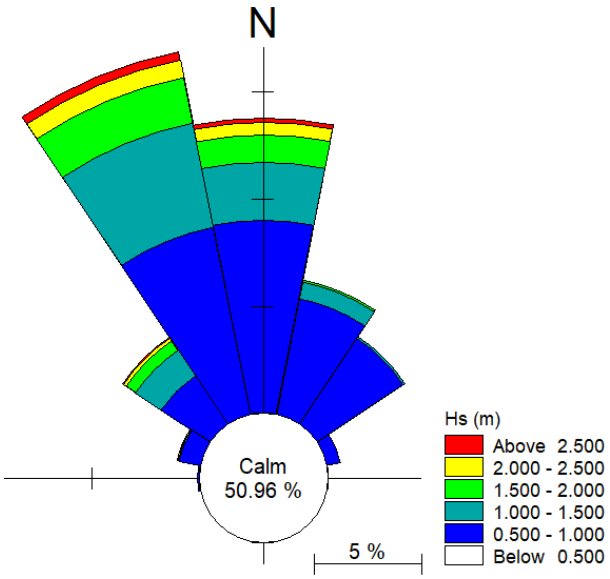


Figure 3. Wave rose for measured data near Nowshahr Port.

In addition to wave measurements, current characteristics were also measured at this location. Figure 4 shows the time series of current speed and direction recorded at this station over several months. The maximum recorded current speed at this station during the measurement period was approximately 0.62 meters per second. To understand the general current pattern based on field measurements, a current rose was plotted based on the data obtained at this station. Figure 5 shows the current rose for measured data at Nowshahr station, which is based on depth-averaged speeds. According to Figure 5, the general current pattern in this region is primarily east-west, with a higher frequency of west-to-east currents compared to east-to-west currents.

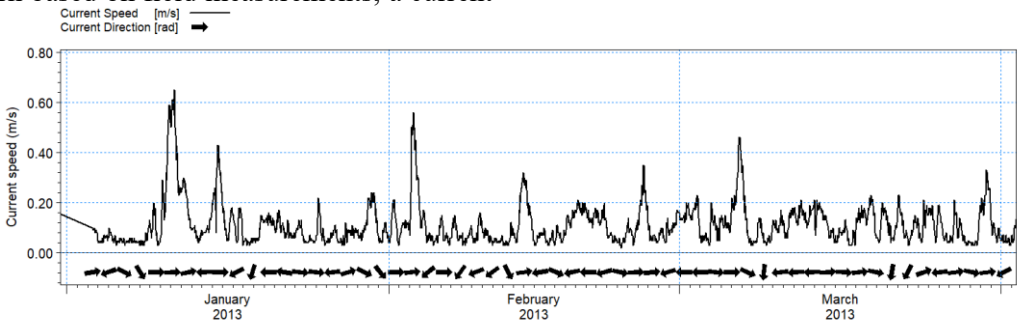


Figure 4. Time series of current speed and direction measured near Noshahr Port for a sample period.

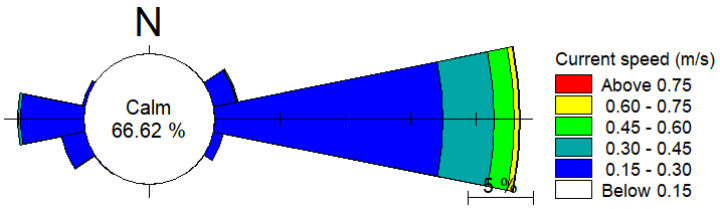


Figure 5. Current rose for measured data near Nowshahr Port.

In this part of the simulations, a triangular mesh was used for the model grid. In this study, the mesh file was generated such that the grid resolution and size were as optimal as possible across the computational domain. The mesh and bathymetry data used for wave generation and propagation analysis are shown in Figure 6. The grid resolution varies between 0.02 and 0.25 degrees in different areas.

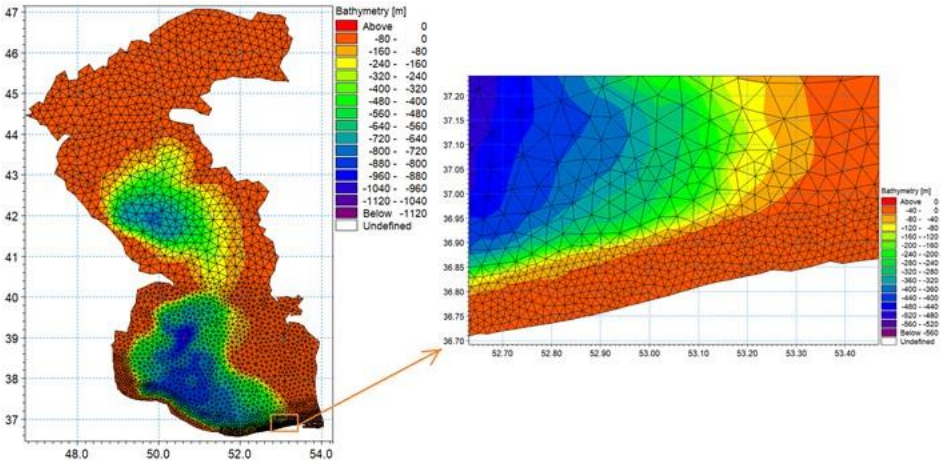


Figure 6. Computational mesh used for large-scale simulations of the Caspian Sea.

3. Results and Discussion

3.1. Sensitivity Analysis of Wave Models to Different Parameters

The results of numerical models are dependent on various factors, such as mesh size, angular division, numerical equation solving accuracy, wave breaking coefficients, bed roughness, wave crest white-capping coefficients, and more. To calibrate numerical models, it is first necessary to assess the impact of highly sensitive factors on the results.

In some regions, refining the computational mesh can enhance accuracy, but it also increases computational costs significantly. If mesh refinement does not yield considerable improvements in results, coarser meshes with lower computational costs are preferable. Figures 8 and 9 compare the results of models with different mesh sizes in deep water and nearshore locations, respectively. As shown, finer meshes do not substantially improve the results, only raising computational costs. Therefore, mesh sizes ranging from 0.02 to 0.25 degrees were used for final calculations.

3.1.1. Sensitivity to Mesh Size

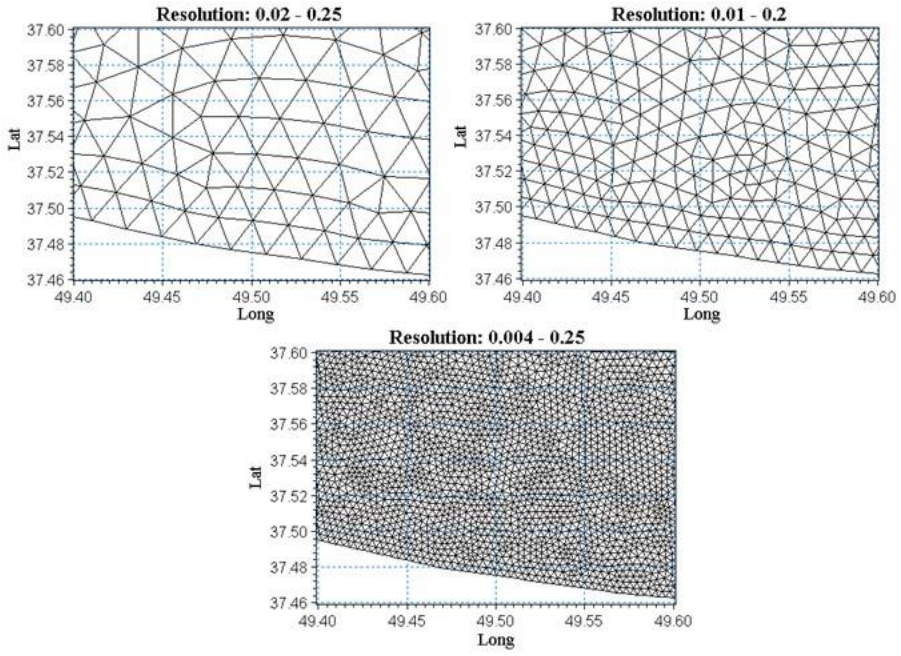


Figure 7. Computational mesh generated with different sizes for sensitivity analysis.

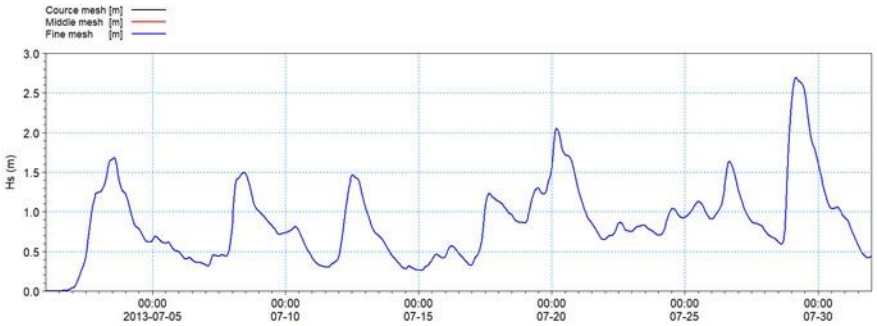


Figure 8. Comparison of model results with different mesh sizes at a deep-water point.

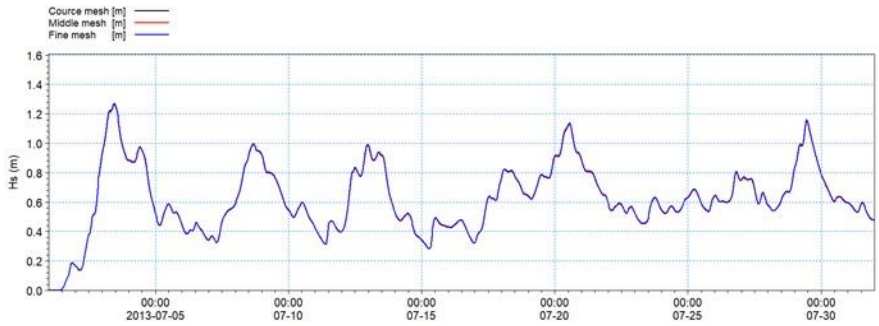


Figure 9. Comparison of model results with different mesh sizes near the coast.

3.1.2. Sensitivity to Angular Divisions

One of the features of spectral wave models is the ability to perform calculations not only on a spatial computational grid but also on a spectral grid. This grid has two dimensions: direction and frequency. In spectral models, users can choose a full directional spectrum or set a minimum and maximum range for it. Figures 10 and 11 compare the results of models with different angular divisions at deep-water and nearshore points. As can be seen, varying the number of angular divisions has little effect on the model output.

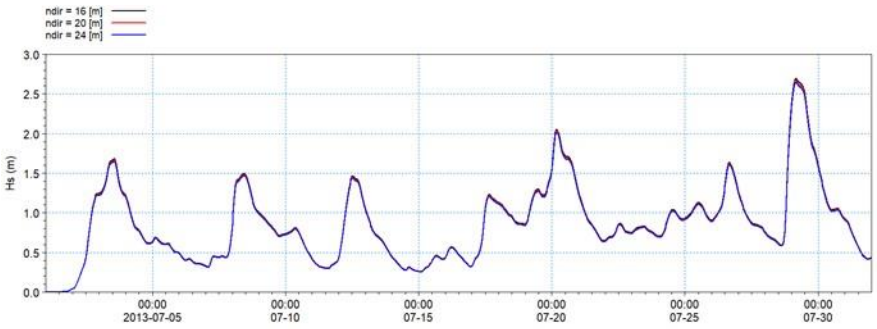


Figure 10. Comparison of model results with different angular divisions at a deep-water point.

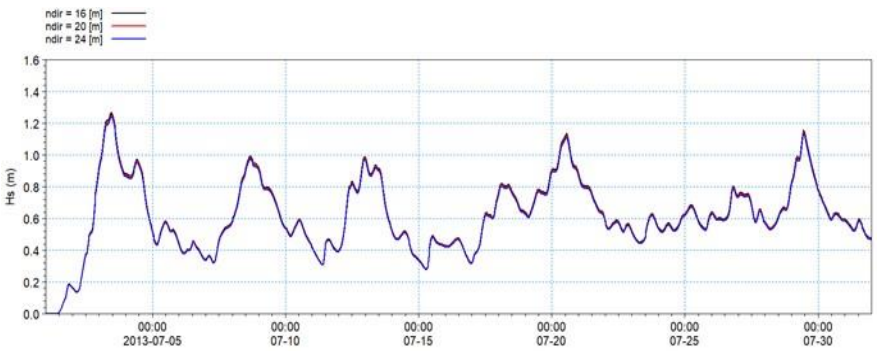


Figure 11. Comparison of model results with different angular divisions near the coast.

3.1.3. Sensitivity Analysis of Bed Roughness Coefficient

One of the factors affecting waves in shallow regions is bed roughness. In the MIKE-SW model, the Nikuradse roughness coefficient (kn) can be applied to account for bed roughness [16]. The value of this coefficient can be selected by the user. For the sensitivity analysis, values of 0.04 (the default in the model), 0.4, and 0.004 were chosen, and the model was run for each case. The simulated wave heights with different Nikuradse roughness coefficients are compared in Figures 12 and 13 for deep water and nearshore locations, respectively. As shown, changing this coefficient has no effect in deep water, but it can be used as one of the main calibration factors in shallow water areas.

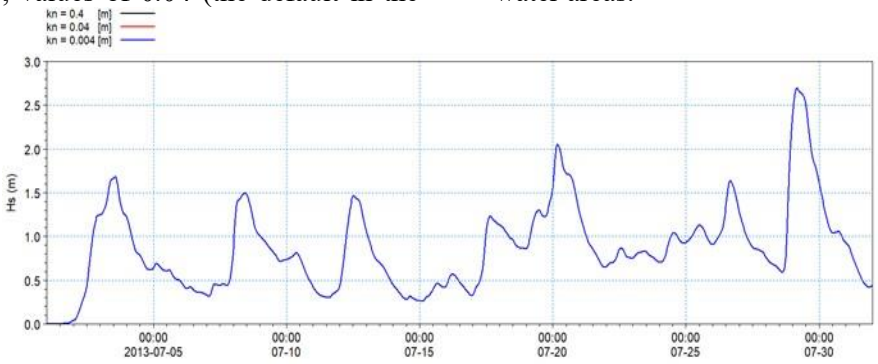


Figure 12. Comparison of model results with different bed roughness coefficients at a deep-water point.

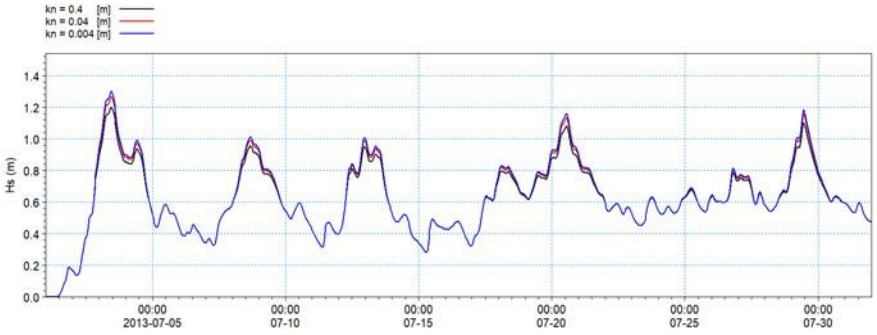


Figure 13. Comparison of model results with different bed roughness coefficients near the coast.

3.1.4. Sensitivity Analysis of Wave Breaking Coefficients in Shallow Water

In wave formation and propagation calculations, wave breaking is a critical phenomenon that affects the distribution of wave heights. Wave breaking occurs when waves enter shallow areas, and the water depth cannot support the wave energy. As a result, part of the wave's energy is dissipated. An additional sink term appears in the governing spectral equation to account for this energy loss. In the MIKE21 SW model, this term is based on the relationships provided by Battjes and Janssen [17], which have proven effective in spectral models.

In this model, two coefficients are considered: one to control the energy dissipation rate after wave breaking (parameter α), and the other to control the depth at which wave breaking occurs (parameter γ). Increasing parameter α increases the energy dissipation rate, while increasing parameter γ reduces the wave breaking depth.

3.1.5. Sensitivity Analysis of wave crest whitecaps Coefficients

wave crest whitecaps refers to surface turbulences that cause energy dissipation in deep water and are the primary mechanism controlling wave energy in these regions. The concept of deep-water wave breaking was first introduced by Hasselmann in 1974, and its equations were revised by Komen et al. in 1984 [18][19]. In the MIKE21-SW model, two parameters C_{dis} and δ are provided for direct or indirect control of energy dissipation. The range of coefficients $C_{dis} \approx 2.36 \times 10^{-5}$ and $\delta \approx 0{\sim}1$ is available. In the MIKE SW model, the default values of these parameters $C_{dis} = C_{dis}\ (1/\widetilde{s_{PM}})^4$ and $\Delta_{dis} = \delta$ are set to 4.5 and 0.5, respectively. Sensitivity analysis was conducted by varying these two parameters C_{dis} and Δ_{dis}. Different combinations of values for C_{dis} and Δ_{dis} were tested to analyze the sensitivity of wave height results.

In Figures 14 and 15, a comparison of the wave heights derived from various parameters of wave crest

whitecaps at a deep-water buoy and nearshore location is presented. As can be observed, the simulated wave height is significantly influenced by parameter C_{dis}, while it shows minimal sensitivity to the weight parameter Δ_{dis}. It is evident that while parameter C_{dis} remains constant, considerable changes in parameter Δ_{dis} have not led to a substantial variation in wave height. However, since parameter C_{dis} directly controls the energy dissipation, it is observed that a reduction in this parameter has resulted in a notable increase in wave height.

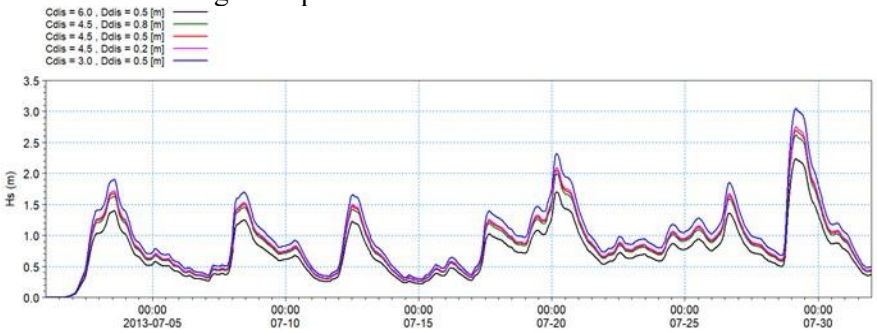


Figure 14. Comparison of wave height results of models with different wave crest whitecap coefficients at a point in deep water.

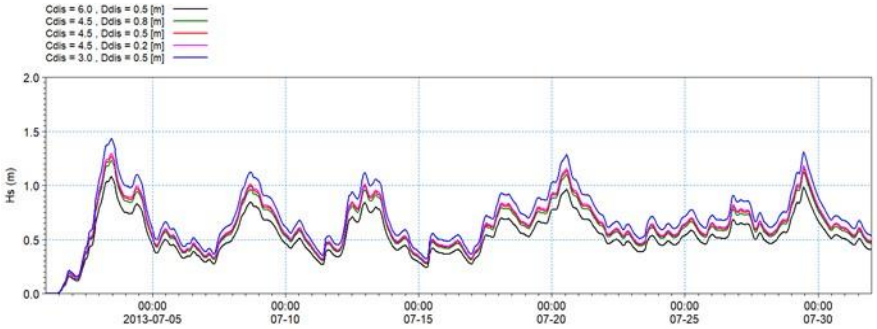


Figure 15. Comparison of wave height results of models with different wave crest whitecap coefficients at a point near the shore.

To further investigate the sensitivity of wave crest whitecap parameters, the effect of these parameters on wave period was also analyzed. In Figures 16 and 17, the changes in wave period $(T_{m,02})$ for the aforementioned scenarios are compared. As observed, the wave period's sensitivity to these parameters varies, with the period being slightly more sensitive to parameter Δ_{dis} compared to parameter C_{dis}. It is clear that an increase in parameter Δ_{dis} directly results in an increase in the wave period. For instance, changing parameter Δ_{dis} from 0.2 to 0.8 causes an increase of 0.5 to 0.8 seconds in the wave period. This analysis demonstrates that, compared to default conditions, the period can be adjusted by approximately half a second through the calibration of wave crest whitecap parameters. Additionally, regarding wave height, it is possible to influence wave characteristics by up to 30% using the calibration of whitecap parameters.

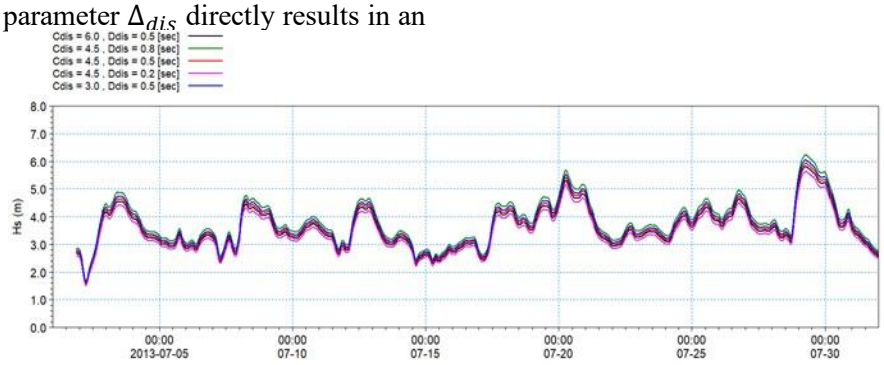


Figure 16. Comparison of wave period results of models with different wave crest whitecap coefficients at a point in deep water.

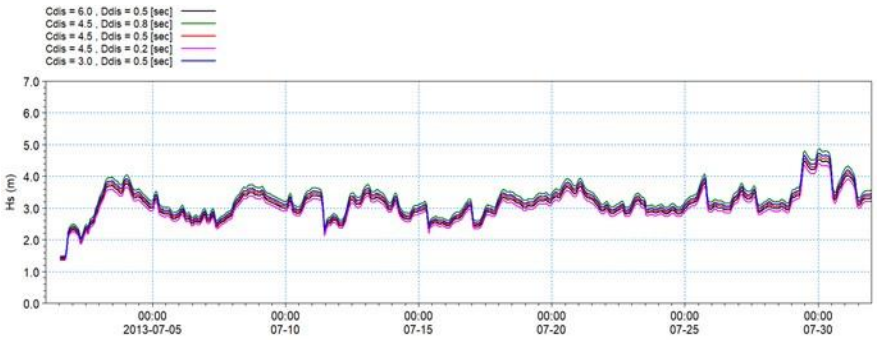


Figure 17. Comparison of wave period results of models with different wave crest whitecap coefficients at a point near the shore.

3.2. Sensitivity Analysis of the Flow Model to Various Parameters

In this section, the sensitivity of the flow model results to different factors such as computational grid size, numerical accuracy, the effect of the Coriolis force, horizontal eddy viscosity coefficient, tidal effects, bed roughness coefficient, and wind friction coefficient has been examined. The various results for the model's runtime at the ADCP field measurement location in Nowshahr have been compared. The effect of each parameter will be discussed further.

3.2.1. Sensitivity Analysis to Computational Grid Size

Figure 18 shows the comparison of changes in flow velocity against Nowshahr port. As observed, refining the computational grid did not result in any significant changes in the results but only increased the computational cost. Therefore, a grid size between 0.02 to 0.25 degrees was used for the final computations.

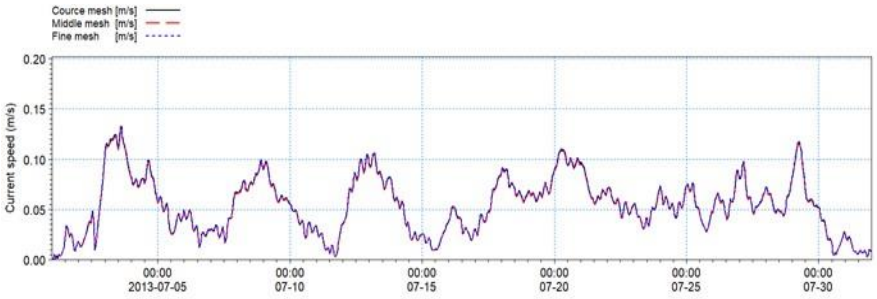


Figure 18. Comparison of flow model results with different computational grids at the ADCP measurement point in Nowshahr.

3.2.2. Sensitivity Analysis to the Effect of the Coriolis Force

The Coriolis force is a pseudo-force that causes the deflection of moving objects from a straight path as viewed from a rotating system, such as Earth. The effects of this force can clearly be seen in determining the direction of atmospheric fronts and planetary currents. Perhaps the most significant example of the Coriolis effect on large dynamic systems is the ocean, where it leads to changes in current velocities. To investigate the Coriolis effect on flow changes, two models were considered: the first without considering the Coriolis force and the second incorporating a variable Coriolis force across the entire modeled area. The results are shown as a time series of current velocities near Nowshahr in Figure 19. This figure shows that ignoring the Coriolis force can significantly affect current flow and water surface levels. Therefore, given the geographic location of the Caspian Sea and the importance of the Coriolis force in this region, it was decided to consider the Coriolis force as variable in space. It is worth mentioning that this option does not increase the computational cost compared to other models, but it provides more confidence in the accuracy of the results.

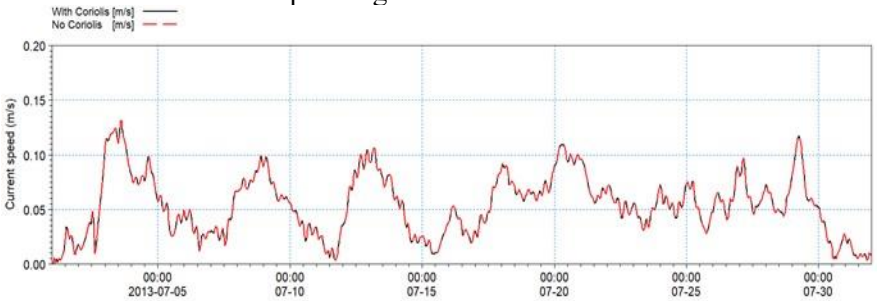


Figure 19. Comparison of flow model results with and without considering the Coriolis effect at the ADCP measurement point in Nowshahr.

3.2.3. Sensitivity Analysis of the Effect of Horizontal Eddy Viscosity Coefficient

In many applications, eddy viscosity is used as a constant. In other cases, the Smagorinsky model is used. The Smagorinsky coefficient C_s should be selected within the range of 0.25 to 1. However, the minimum eddy viscosity can be chosen as zero, but due to its non-physical nature, this is generally avoided. The default value for this coefficient in the model is 0.28. By changing this value to 0.2 and 0.4, their effects on the flow results were evaluated. The result of the modeling, shown as the flow velocity time series near Nowshahr, is presented in Figure 20. As seen in the figure, there is no significant difference between the results from the two models. Therefore, this coefficient cannot be used for model calibration.

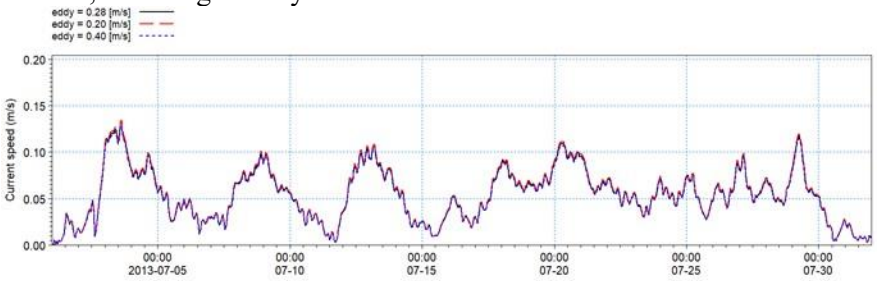


Figure 20. Comparison of Flow Model Results with Different Eddy Viscosity Coefficients at the ADCP Measurement Point in Nowshahr.

3.2.4. Sensitivity Analysis of the Tidal Effects

To examine this effect, two models with and without tidal effects were employed. The time series chart of the flow and water level results for the two conditions, with and without tidal effects near Nowshahr, is shown in Figure 21. This figure indicates that tidal effects do not influence the flow results. Therefore, tidal effects were disregarded in the final model.

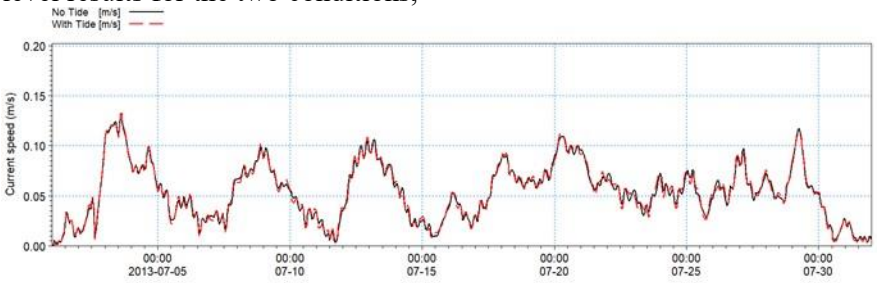


Figure 21. Comparison of Flow Model Results with and without Tidal Effects at the ADCP Measurement Point in Nowshahr.

3.2.5. Sensitivity Analysis of the Wind Friction Coefficient

By changing the value of the wind friction coefficient, the shear stress exerted by the wind on the water surface changes, thus altering the flow velocity. This is particularly significant at high wind speeds, which can cause increased flow velocities. This coefficient can either be constant (default value 0.001255) or variable (a function of wind speed, with 0.001255 for a 3 m/s wind and 0.002455 for a 25 m/s wind according to the default model). Between these two speeds, the coefficient is selected linearly. For the sensitivity analysis, different coefficients with various values were examined:

- 0.002455 and 0.001255 for wind speeds of 7 and 25 m/s (default)
- 0.002455 and 0.001255 for wind speeds of 3 and 15 m/s
- 0.002455 and 0.001255 for wind speeds of 3 and 15 m/s

Figure 22 shows a comparison of the flow velocity variations in models with different wind friction coefficients at a depth of 13 meters opposite the Nowshahr Port. As seen in the figure, the magnitude of the marine currents depends on the wind friction coefficient values.

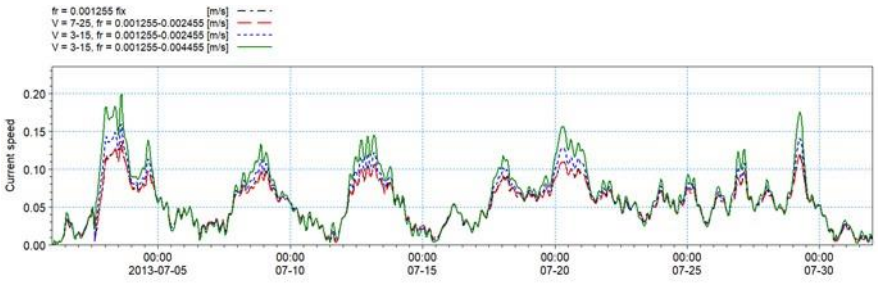


Figure 22. Comparison of Flow Model Results with Different Wind Friction Coefficients at the ADCP Measurement Point in Nowshahr.

4. Conclusion

In this study, after modeling waves and currents in the MIKE software, a sensitivity analysis of various parameters in the wave and current model was conducted. The results were also compared with field measurements. The wave section results indicated that among the parameters studied, the parameters of the number of angular divisions in the spectrum, the accuracy of the computational method, and shallow water wave breaking had little effect on the output results in the southern Caspian Sea and could not be used for model calibration. Reducing the computational grid size had a certain impact on the accuracy of the results up to a point, but beyond that, it only increased computational cost. This parameter is also not suitable for calibration, and the grid size should be optimally chosen so that spatial discretization does not affect the results. The bed roughness coefficients and the wave crest capping each had a moderate effect on the results and can be considered as key parameters in the model calibration process. Moreover, the current section results showed that the accuracy of numerical computations, the effect of Coriolis force, horizontal eddy viscosity coefficient, tidal effects, bed roughness coefficient, and wind friction coefficient were analyzed. Among the parameters examined, the accuracy of numerical computations, the eddy viscosity coefficient, and tidal effects did not have significant impacts on the output results. The Coriolis force, considered variable across the entire model, did not have a major effect either. The bed roughness coefficient and wind friction coefficient influenced the results and can be used for model calibration.

References

[1] Iooss, B., & Lemaître, P. (2015). A review on global sensitivity analysis methods. *Uncertainty management in simulation-optimization of complex systems: algorithms and applications*, 101-122.

[2] Liu, Z., & Soares, C. G. (2023). Sensitivity analysis of the cage volume and mooring forces for a gravity cage subjected to current and waves. *Ocean Engineering*, *287*, 115715.

[3] Beels, C., Troch, P., De Backer, G., Vantorre, M., & De Rouck, J. (2010). Numerical implementation and sensitivity analysis of a wave energy converter in a time-dependent mild-slope equation model. *Coastal Engineering*, *57*(5), 471-492.

[4] DAO, N. X., ADITYAWAN, M. B., & TANAKA, H. (2013). Sensitivity analysis of shore-parallel canal for tsunami wave energy reduction. *Journal of Japan Society of Civil Engineers, Ser. B3 (Ocean Engineering)*, *69*(2), I_401-I_406.

[5] Nekouee, N., Hamidi, S. A., & Etemadi, R. (2015). Sensitivity analysis of numerical wave predictions models, considering wind and geometry effects in rectangular lakes. *Ocean Engineering*, *104*, 549-557.

[6] Wu, C. C., & Emanuel, K. A. (1995). Potential vorticity diagnostics of hurricane movement. Part 1: A case study of Hurricane Bob (1991). *Monthly weather review*, *123*(1), 69-92.

[7] Bastidas, L. A., Knighton, J., & Kline, S. W. (2016). Parameter sensitivity and uncertainty analysis for a storm surge and wave model. *Natural Hazards and Earth System Sciences*, *16*(10), 2195-2210.

[8] Liu, Z., & Guo, H. (2018). Sensitivity analysis of steep wave riser with internal flow. *Journal of Marine Science and Technology*, *26*(4), 7.

[9] Han-bao, C., Ya-nan, X., & Yong-zhou, C. (2021). Sensitivity analysis of wave direction in wave numerical model. In *IOP Conference Series: Earth and Environmental Science* (Vol. 621, No. 1, p. 012076). IOP Publishing.

[10] Dezvareh, R., & Shafaghat, M. (2020). Predicting the sediment rate of Nakhilo Port using artificial intelligence. *International Journal Of Coastal, Offshore And*

Environmental Engineering (ijcoe), *5*(2), 41-49.

[11] Dezvareh, R. (2019). Providing a new approach for estimation of wave set-up in Iran coasts. *Research in marine sciences*, *4*(1), 438-448.

[12] Dezvareh, R., Bargi, K., & Moradi, Y. (2012). Assessment of Wave Diffraction behind the Breakwater Using Mild Slope and Boussinesq Theories. *International Journal of Computer Applications in Engineering Sciences*, *2*(2).

[13] Shafaghat, M., & Dezvareh, R. (2021). Support vector machine for classification and regression of coastal sediment transport. *Arabian Journal of Geosciences*, *14*(19), 2009.

[14] Gholizadeh, S., Dezvareh, R., & Kiani, A. (2024). Comparison of different support vector machine kernels for monitoring of the last decade of the Iranian part of eastern Caspian Lake. *International Journal Of Coastal, Offshore And Environmental Engineering (ijcoe)*, *9*(1), 55-63.

[15] Warren, I. R., & Bach, H. (1992). MIKE 21: a modelling system for estuaries, coastal waters and seas. *Environmental software*, *7*(4), 229-240.

[16] Nodeh, H. M., Dezvareh, R., & Yousefifard, M. (2024). Numerical Analysis of the Effects of Rubble Mound Breakwater Geometry Under the Effect of Nonlinear Wave Force. *Arabian Journal for Science and Engineering*, *49*(4), 5767-5783.

[17] Farhadzadeh, A., Kobayashi, N., & Gravens, M. B. (2012). Effect of breaking waves and external current on longshore sediment transport. *Journal of waterway, port, coastal, and ocean engineering*, *138*(3), 256-260.

[18] Hasselmann, K. (1974). On the spectral dissipation of ocean waves due to white capping. *Boundary-Layer Meteorology*, *6*, 107-127.

[19] Komen, G. J., Hasselmann, S., & Hasselmann, K. (1984). On the existence of a fully developed wind-sea spectrum. *Journal of physical oceanography*, *14*, 1271-1285.

[20] Dadashzadeh, M., Parsa, J., & Mojtahedi, A. (2020). Investigation over the interaction of Lake Urmia wave pattern and causeway using meteorological models and computational fluid dynamics. *Journal of Oceanography*, *11*(41), 49-61.